

The Canada-UK Deep Submillimetre Survey VIII: Source Identifications in the 3-hour field

Dave Clements^{1,2}, Steve Eales^{1*}, Kris Wojciechowski¹, Tracy Webb³,
Simon Lilly⁴, Loretta Dunne¹, Rob Ivison⁵, Henry McCracken⁶,
Min Yun⁷, Ashley James¹, Mark Brodwin⁸, Olivier Le Fèvre⁹ and Walter Gear¹

¹*Department of Physics and Astronomy, Cardiff University, P.O. Box 913, Cardiff CF24 3YB, UK*

²*Imperial College, Blackett Laboratory, Prince Consort Road, London SW7 2BZ*

³*Sterrewacht Leiden, Postbus 9513, 2300 RA Leiden, the Netherlands*

⁴*Institut für Astronomie, ETH Hönggerberg, HPF G4.1, CH-8093, Zürich, Switzerland*

⁵*Astronomy Technology Centre, Royal Observatory, Blackford Hill, Edinburgh EH9 3HJ, UK*

⁶*University of Bologna, Department of Astronomy, via Ranzani 1, 40127 Bologna, Italy*

⁷*Department of Physics and Astronomy, University of Massachusetts, 640 Lederle Graduate Research Center, Amherst, MA01003, USA*

⁸*Department of Astronomy, University of Toronto, 60 St. George Street, Toronto, Ontario, Canada, M5S 3H8*

⁹*Labatoire d'Astrophysique de Marseilles, Traverse du Siphon, 13376 Marseille Cedex 12, France*

9 November 2018

ABSTRACT

We present optical, near-infrared and radio observations of the 3-hour field of the Canada-UK Deep Submillimetre Survey. Of the 27 submillimetre sources in the field, nine have secure identifications with either a radio source or a near-IR source. We show that the percentage of sources with secure identifications in the CUDSS is consistent with that found for the bright ‘8 mJy’ submillimetre survey, once allowance is made for the different submillimetre and radio flux limits. Of the 14 secure identifications in the two CUDSS fields, eight are VROs or EROs, five have colours typical of normal galaxies, and one is a radio source which has not yet been detected at optical/near-IR wavelengths. Eleven of the identifications have optical/near-IR structures which are either disturbed or have some peculiarity which suggests that the host galaxy is part of an interacting system. One difference between the CUDSS results and the results from the 8-mJy survey is the large number of low-redshift objects in the CUDSS; we give several arguments why these are genuine low-redshift submillimetre sources rather than being gravitational lenses which are gravitationally amplifying a high- z submillimetre source. We construct a $K - z$ diagram for various classes of high-redshift galaxy and show that the SCUBA galaxies are on average less luminous than classical radio galaxies, but are very similar in both their optical/IR luminosities and their colours to the host galaxies of the radio sources detected in μ Jy radio surveys.

Key words: submillimetre-dust-galaxies:evolution-galaxies:formation

1 INTRODUCTION

The luminous high-redshift dust sources discovered by the SCUBA submillimetre and MAMBO millimetre surveys (Smail, Ivison & Blain 1997; Hughes et al. 1998; Barger et al. 1998; Eales et al. 1999; Bertoldi et al. 2000,2001) are almost certainly of great significance for our understanding of galaxy formation. The ultimate energy source in these objects is hidden by dust but the two obvious possibilities

are that (1) the dust is being heated by a hidden active nucleus or (2) the dust is being heated by a luminous population of stars. The first of these can now largely be ruled out because of the failure of the XMM/Newton and Chandra telescopes to detect strong X-ray emission from many of the dust sources (e.g. Ivison et al. 2002; Almaini et al. 2003; Waskett et al. 2003a; Alexander et al. 2003). Estimates of the star-formation rates necessary to produce the dust luminosity can be as high as $6 \times 10^3 M_{\odot} \text{ year}^{-1}$ (Smail et al. 2003), enough to produce the stellar population of a massive galaxy in $\sim 10^8 - 10^9$ years. Many authors have concluded that these dust sources are the ancestors of present-day el-

* Comments or queries about the paper should be sent to Steve Eales at sae@astro.cf.ac.uk

lptical galaxies, basing their arguments on estimates of the star-formation rate in the population as a whole (Smail, Ivison and Blain 1997; Hughes et al. 1998; Blain et al. 1999), on estimates of the contribution of the sources to the extragalactic background radiation (Eales et al. 1999), and on comparisons of the space-density of the SCUBA/MAMBO sources (henceforth SMS) with the space-density of ellipticals in the universe today (Scott et al. 2002; Dunne, Eales and Edmunds 2003).

In view of the probable significance of this population, it is of great importance to determine the optical counterparts to the SMSs and measure their redshifts. If the SMSs are the ancestors of present-day elliptical galaxies, what do the properties of the SMSs tell us about how elliptical galaxies form? There are two rival theories of the birth of an elliptical. In the older of these (Eggen, Lynden-Bell and Sandage 1962; Larson 1975), an elliptical forms when an individual gas cloud in the early universe collapses, most of the galaxy's stars forming during the collapse. In the modern theory, the elliptical forms as the result of a sequence of galaxy mergers. This may occur over a relatively long period of cosmic time, with a burst of star formation being triggered during each merger, or it may occur as the result of a few mergers at high redshift (Cole et al. 2000; Percival et al. 2003). If an SMS does represent one of these galaxy-building bursts of star formation, the redshifts of the SMSs are clearly crucial for determining the correct model for elliptical formation. If the older theory is correct, for example, the redshift distribution of the SMSs should probably have a pronounced peak, corresponding to the epoch in which most ellipticals formed.

Unfortunately one of the major problems in understanding this population has been the difficulty of determining the optical counterparts and measuring the redshifts of the SMSs. The obstacles here are the large errors on the positions of the SMSs, which often make it difficult to determine the optical/IR counterpart to the SMS, and the faintness of these counterparts, which make it difficult to measure a redshift. Until recently, the recourse of most groups has been to try to detect the SMSs at radio wavelengths, since the surface density of radio sources in deep VLA radio surveys is low enough that it is possible to be confident that apparent radio counterparts to SMSs are not chance coincidences. Once an SMS has been securely identified with a radio source, the accurate radio position can be used to determine the optical/IR counterpart. Furthermore, Carilli and Yun (1999) pointed out that, if SMSs are star-forming galaxies like those in the universe today, it is possible to estimate the redshift of the SMS from the ratio of radio to submillimetre flux. Fortunately, a significant fraction of the SMSs are also faint radio sources. Ivison et al. (2002), for example, found that 60% of the SMSs in the '8 mJy' SCUBA survey are also radio sources. The optical objects found at the radio positions are usually faint, often appear to be merging or interacting systems (Lilly et al. 1999; Ivison et al. 2000; Webb et al. 2003a), and often have very red optical-infrared (I-K) colours, with a significant number being as red as the 'Extremely Red Objects' (Ivison et al. 2002; Webb et al. 2003a).

Recently Chapman et al. (2003a) have taken a major step forward by measuring the redshifts for a significant number of SMSs with accurate radio positions. Rather sur-

prisingly, given the dust in these objects, this group succeeded in detecting Lyman α and other *UV* lines with the Keck Telescope from 10 SMSs. The redshifts they have measured lie in the range $0.8 < z < 4$, although because of the requirement for accurate radio positions, and because the ratio of radio to submillimetre flux is expected to fall with redshift (Carilli and Yun 1999), this distribution may well be skewed towards low redshifts. Nevertheless, the wide range of redshifts is in better agreement with modern ideas about the formation of ellipticals than with the older theory. The result that a large fraction of SMSs are merging or interacting systems is also in better agreement with these ideas.

In this paper we describe the results of our attempts to determine the optical and counterparts to the SMSs in the 3-hour field of the Canada-UK Deep Submillimetre Survey. Our cosmological assumptions in this paper are a concordance universe with $\Omega_{\Lambda} = 0.7$ and $\Omega_{\text{M}} = 0.3$ and a Hubble constant of $75 \text{ km s}^{-1} \text{ Mpc}^{-1}$.

2 THE SURVEY

The Canada-UK Deep Submillimetre Survey (Eales et al. 1999) is one of the largest of the deep SCUBA submillimetre surveys. The basic survey consists of deep $850\mu\text{m}$ images of two fields at a right ascension of 3^{h} and 14^{h} . Each field is about $6 \times 8 \text{ arcmin}^2$ in size and the 3σ sensitivity at $850\mu\text{m}$ is about 3 mJy. This is the eighth paper describing the results from the survey. The first two papers (Eales et al. 1999; Lilly et al. 1999) describe the submillimetre and optical results from initial surveys of parts of the two fields, together with the results from a survey of a third smaller field at a right ascension of 10^{h} . Paper III (Gear et al. 2000) describes millimetre interferometry of the brightest source in the 14^{h} field. Paper IV (Eales et al. 2000) describes the submillimetre observations of the 14^{h} field. Paper V (Webb et al. 2003b) describes an investigation of the cross-clustering between the SCUBA sources and the Lyman break galaxies in the two fields. Paper VI (Webb et al. 2003c; henceforth W2003) describes the submillimetre survey of the 3-hour field. Paper VII (Webb et al. 2003a) describes the follow-up optical/IR observations of the 14-hour field. This paper describes the follow-up optical/IR observations of the 3-hour field. A final paper (Eales et al., in preparation) will describe an investigation of galaxy evolution in the submillimetre waveband using the results from the survey. The 27 sources in the 3-hour field (W2003) are listed in Table 1.

3 THE OBSERVATIONS

This field was originally observed in the optical and infrared wavebands as part of the Canada-France Redshift Survey (Lilly et al. 1995). It has been observed in the mid-infrared waveband with the Infrared Space Observatory (W2003; Flores et al. 2003) and in the X-ray waveband with XMM/Newton (Waskett et al. 2003a). To determine the counterparts to the SCUBA sources, we have used a new radio image obtained with the VLA, deep infrared observations made with the UK Infrared Telescope (UKIRT) and with the Canada-France Hawaii Telescope (CFHT), and

Table 1. Submillimetre Sources

(1) Name	(2) RA (J2000)	(3) Dec (J2000)	(4) S/N	(5) $S_{850\mu\text{m}}/\text{mJy}$
CUDSS 3.1	03 02 44.55	00 06 34.5	7.4	10.6±1.4
CUDSS 3.2	03 02 42.80	00 08 1.50	6.7	4.8±0.7
CUDSS 3.3	03 02 31.15	00 08 13.5	6.4	6.7±1.0
CUDSS 3.4	03 02 44.40	00 06 55.0	6.2	8.0±1.3
CUDSS 3.5	03 02 44.40	00 08 11.5	5.8	4.3±0.7
CUDSS 3.6	03 02 36.10	00 08 17.5	5.4	3.4±0.6
CUDSS 3.7	03 02 35.75	00 06 11.0	5.3	8.2±1.5
CUDSS 3.8	03 02 26.55	00 06 19.0	5.0	7.9±1.6
CUDSS 3.9	03 02 28.90	00 10 19.0	4.6	5.4±1.2
CUDSS 3.10	03 02 52.50	00 08 57.5	4.5	4.9±1.1
CUDSS 3.11	03 02 52.90	00 11 22.0	4.0	5.0±1.3
CUDSS 3.12	03 02 38.70	00 10 26.0	4.0	4.8±1.2
CUDSS 3.13	03 02 35.80	00 09 53.5	3.8	4.1±1.1
CUDSS 3.14	03 02 25.78	00 09 7.50	3.5	5.1±1.5
CUDSS 3.15	03 02 27.60	00 06 52.5	3.5	4.4±1.3
CUDSS 3.16	03 02 35.90	00 08 45.0	3.4	2.8±0.8
CUDSS 3.17	03 02 31.65	00 10 30.5	3.4	5.0±1.5
CUDSS 3.18	03 02 33.15	00 10 19.5	3.3	3.9±1.2
CUDSS 3.19	03 02 43.95	00 09 52.0	3.2	3.3±1.0
CUDSS 3.20	03 02 53.30	00 09 40.0	3.2	3.4±1.1
CUDSS 3.21	03 02 25.90	00 08 19.0	3.1	3.8±1.2
CUDSS 3.22	03 02 38.40	00 06 19.5	3.1	3.1±1.0
CUDSS 3.23	03 02 54.00	00 06 15.5	3.1	5.8±1.9
CUDSS 3.24	03 02 56.80	00 08 8.00	3.0	5.1±1.7
CUDSS 3.25	03 02 38.65	00 11 12.0	3.0	4.1±1.4
CUDSS 3.26	03 02 35.10	00 09 12.5	3.0	3.6±1.2
CUDSS 3.27	03 02 28.56	00 06 37.5	3.0	4.0±1.3

(1) Source name. (2) & (3) Position (RA and Dec) in J2000 coordinates (4) Signal-to-noise with which the submillimetre source was detected (W2003), (5) Flux at 850 μm of source in mJy.

optical observations made with the CFHT and the Hubble Space Telescope.

3.1 Radio Observations

We observed this field at 1.4 GHz with the VLA in both the A and B configuration. The reduced radio image and the source catalogue will be presented elsewhere. The noise on the final image was 11 μJy .

3.2 Infrared Observations

We obtained two complementary datasets for the field: observations in the K-band with the infrared camera (UFTI) on the UKIRT and observations in the K'-band with the infrared camera (CFHTIR) on the CFHT.

3.2.1 UKIRT Observations

The UFTI camera on the UKIRT uses a tip-tilt-correcting secondary mirror to deliver images with high angular resolution to an array with small pixels (0.0906 arcsec). It can thus provide very deep high resolution images, which are useful not only for identifying the CUDSS sources but also for providing morphological information which may help us to understand their origin and nature. The small pixel size of the UFTI, however, has the drawback that many fields would need to be observed to cover completely the region

of the submillimetre survey. At present, we have obtained UFTI images of 18 of the 27 sources.

We observed the 3-hour field on the nights 9, 10, 12, 18 and 23 January 2000 and 20-22 October 2001 in the K-band. The camera has a 1024² HgCdTe focal-plane array which gives a field-of-view of 93 \times 93 arcsec². Our observations consisted typically of a series of nine short (120s in the first run, 80s in the second) integrations, made in a semi-random pattern over a 9 \times 9 arcsec² area of sky. After the first group of nine observations, the telescope was offset by 1 arcsec, and the same pattern was repeated. Each of these cycles consists of 18 minutes of integration time (12 minutes for the later run). We carried out between six and 10 of these cycles for each target. To calibrate our observations, we observed stars from the list of UKIRT faint photometric standards several times each night, principally FS7, FS11 and FS30.

We carried out the reduction of the data from each nine-integration cycle using the ORACDR pipeline system, which contains procedures for sky subtraction, flat fielding, the removal of bad pixels, and the coaddition and registration of the individual observations. The output of the pipeline is a fully-reduced image of the data from each cycle. For each target, we then aligned and added the images produced by the pipeline, using routines from the STARLINK CCDPACK library. The faintest objects visible on the final images have magnitudes between K \sim 20.5 and K \sim 21.5.

3.2.2 CFHT Observations

We observed the 3-hour field in the K' band using the new near-infrared camera (CFHTIR) on the CFHT during the period 9-15 Jan 2001. The seeing was typically 0.8-1.0 arcsec. CFHTIR has 1024×1024 pixels, each with a size of 0.211 arcsec, giving a field-of-view of 3.6×3.6 arcmin. We covered two thirds of the area of the 3-hour submillimetre survey with a mosaic of 30-second exposures. We reduced the data using IRAF routines (see Webb et al. 2003a for more information), producing a single image covering 23 of the 27 CUDSS sources. The total integration time at a typical point in the image is 2.7 hours and the faintest visible objects have $K \sim 21.6$.

3.2.3 Deeper Images

As a result of these observations, there was often more than one image of a CUDSS source. In order to obtain as deep an image as possible, we coadded the images. We did this using standard procedures within the STARLINK library. We first extracted the relevant section of the large CFHT image, binned the UFTI image so that it had pixels of the same size as the CFHT image, aligned the images using objects visible on both images, and scaled the images onto a common photometric scale. We then measured the noise on each image, and then added the images using as weights the inverse square of the measured noise. We astrometrically calibrated the final images using objects which were visible in both the K-band images and in the Canada-France Deep Field I-band image (see below). The good agreement between the radio and K-band positions (§4) implies that in most cases the accuracy of the K-band positions is better than 0.5 arcsec.

The final images are shown in Figure 1. We used the SEXTRACTOR image-detection package to produce catalogues of sources for use in our identification analysis. We obtained K-band magnitudes of each potential identification using a circular aperture with a diameter of 3 arcsec.

3.3 Optical Observations

The three-hour field was observed in the optical waveband as part of the Canada-France Deep Fields Survey (CFDF, McCracken et al. 2001). The images obtained as part of this survey consisted of U, B, V and I-band images, each covering an area of 0.25 degrees², and reaching a 3σ limiting AB magnitude of 26.98, 26.38, 26.40, and 25.62, respectively. We used the CFDF images to obtain optical magnitudes for the potential identifications found on the K-band image. In all cases, we used the same 3-arcsec aperture as we had used to measure the K-band magnitudes. The CFDF I-band image of each CUDSS source is shown alongside the K-band image in Figure 1.

For a few of the CUDSS sources there are images taken with the Hubble Space Telescope (HST). Brinchman et al. (1998) obtained three images with the Wide Field and Planetary Camera 2 (WFPC2) in which CUDSS sources fall. These images were taken through the F814W filter and had an integration time of 6700s. We have also obtained a few WFPC2 images specifically to follow up the CUDSS sources. These images were also taken through the F814W filter and had an integration time of 7000s. The HST data that exists

for the CUDSS fields is described in more detail in Webb et al. (2003a).

Note that optical and IR magnitudes given in this paper are based on the Vega zeropoints unless otherwise stated.

4 IDENTIFICATION PROCEDURE

The biggest problem in determining the optical counterparts to the SCUBA sources are the large errors in the positions of the sources. The size of the errors is poorly known because of the uncertain effect on the positions of nearby faint sources which are too faint to be detected individually. Various authors have tried to model this effect (Eales et al. 2000; Hogg 2001; Scott et al. 2002). Eales et al. (2000), for example, carried out an investigation of the positional errors in the CUDSS, using two different methods. They added artificial sources to the real SCUBA images and then compared the positions determined by the source-detection algorithm to the true positions. They also carried out a full-scale Monte-Carlo simulation of one of the CUDSS fields and compared the input and output positions of the sources. They concluded that between 10 and 20% of CUDSS sources have measured positions which differ from the true position by >6 arcsec. Scott et al. (2002) have also examined the effect of adding artificial sources onto their real SCUBA maps. They concluded that the mean positional error in their '8 mJy survey' is $\simeq 3-4$ arcsec. Since the size of the errors is poorly known, it is impossible to use Bayesian statistical techniques (e.g. Sutherland and Saunders 1990). Instead, we and others have adopted the frequentist technique of looking for objects close to the SCUBA position and then estimating the probability of that object being a chance coincidence (e.g. Lilly 1999; Ivison et al. 2002; Serjeant et al. 2003).

The first step in the procedure was to select a radius within which to look for possible counterparts to the SCUBA source. We chose a radius of 8 arcsec, for the practical reason that at larger radii we cannot distinguish a genuine association from a chance coincidence. It is possible, of course, that placing this limit on the search radius will have resulted in our missing some genuine associations. Our investigation of the positional errors in the CUDSS (see above) implies that we will have missed $\simeq 5-8\%$ of the associations. However, this estimate is based on simulations. We will show later that we can now empirically estimate the true distribution of positional errors for SCUBA sources (§6). This empirical investigation implies that our earlier estimates of the positional errors for SCUBA sources were too pessimistic.

The most useful image for our identification analysis is the radio image because the surface-density of radio sources is sufficiently low, even at the μ Jy level, that it is possible to determine whether a radio source is genuinely associated with a SCUBA source with high statistical certainty. As the first step in analysis, we looked for sources within 8 arcsec of the SCUBA position with a peak flux brighter than 40μ Jy (3.6σ). There were 11 sources brighter than this limit within 8 arcsec of the 27 CUDSS sources. Any real source should have an angular size at least as large as the angular resolution of the VLA at this frequency (FWHM of 1.4 arcsec), and after analysing the source structures with the AIPS program JMFIT, we eliminated two sources which had structures inconsistent with the VLA beam. The probability of a

source detected at $>3.6\sigma$ within the search area being the result of noise is $\simeq 0.02$. Since we have searched around 27 CUDSS sources, the expected number of false radio sources is $\simeq 0.54$. Therefore, it is possible that one of the nine radio sources is spurious. However, seven of the nine radio sources are coincident with galaxies (see below), and so are definitely genuine. The exceptions are the sources associated with 3.17 and 3.27.

Given that a radio source is genuine, the probability of it not being associated with the SCUBA source is

$$p = 1 - \exp(-d^2\pi n)$$

in which d is the offset between the SCUBA source and the radio position, and n is the surface density of radio sources. We calculated the surface density of radio sources brighter than $40\mu\text{Jy}$ using the source counts from the Hubble Deep Field (Richards et al. 2000). The probabilities and offsets are listed in Table 2. Seven of the radio sources have probabilities of being chance coincidences of $<1\%$. The remaining two have probabilities of being chance coincidences of 3 and 4%. Therefore, all of these radio sources are almost certainly associated with the nine CUDSS sources.

The surface density of objects on the infrared images in Figure 1 is much higher and so we have to use a more sophisticated technique for discriminating between chance coincidences and genuine associations. Since common sense says that a 17th magnitude galaxy two arcsec from the SCUBA position is less likely to be a chance coincidence than a 24th magnitude galaxy (because 17th magnitude galaxies are much rarer than 24th magnitude galaxies), we need to find a statistic which incorporates the magnitude of the possible association. We have used the statistic suggested by Downes et al. (1986) to calculate the probability that a candidate galaxy on an infrared image within 8 arcsec of the SCUBA position is actually unrelated to the SCUBA source:

$$S = 1 - \exp(-d^2\pi n(< m))$$

in which $n(< m)$ is now the surface density of galaxies brighter than the magnitude (m) of the possible association.

The expression above looks like a probability, but it is not because it does not take account of the galaxies on the image which are fainter than the magnitude of the candidate galaxy. If one of these galaxies had been closer to the SCUBA position, it might have had a lower value of S , and therefore in deriving the sampling distribution for S this possibility has to be taken into account. Downes et al. (1986) describe an analytic technique for determining the sampling distribution of S . However, because of the effect of clustering and because images do not always have a uniform depth, it is preferable to use a Monte-Carlo simulation to determine the probability that a candidate identification which is actually physically unrelated to the SCUBA source has a value of S as low as the measured value. We calculated S for each object within 8 arcsec of the SCUBA position, and then used the Monte-Carlo technique described by Lilly et al. (1999) to estimate the probability (P) that a physically unrelated object would have such a low value of S . We have listed in Table 2 all the objects which have values for this probability < 0.3 . As in our earlier paper, we found that the value of P was typically between six and seven times the value of S .

We used the infrared images in preference to the optical images for this analysis, because SCUBA galaxies are generally quite red (Smail et al. 2000; Ivison et al. 2002), and so the infrared images make it possible to discriminate between genuine associations and coincidences with greater statistical precision than is possible with optical images. There are, however, two SCUBA sources for which there is no object close to the SCUBA position visible on the infrared image but for which there is an object visible on the CFDF I-band image. In the case of these two sources, we applied our analysis to the I-band data, although for these sources we calculated P using the analytic relationships in Downes et al. (1986), rather than applying the full Monte-Carlo analysis.

Almost all the CUDSS sources for which there are objects on the infrared images with values of P less than 0.1 also have radio associations. In most cases, the radio sources coincide, to within the positional errors, with the infrared sources. There are only two CUDSS sources which do not have radio associations but which have possible infrared associations. One, CUDSS 3.2, has a value for P of 0.02. The second, CUDSS 3.5, has a value for P of 0.08. If one was considering CUDSS 3.5 in isolation, one would conclude that the galaxy is genuinely associated with the SCUBA source, since the probability of it being a chance projection is only 8%. However, it is not possible to consider the source entirely in isolation. The 3-hour catalogue contains 27 SCUBA sources and, *even if there are no galaxies associated with these SCUBA sources, one expects to find $0.1 \times 27 \simeq 3$ objects on the infrared images with values of $P \simeq 0.1$* . For this reason, we have decided not to classify this galaxy as a secure identification. In Table 2, we have divided possible identifications into two classes. We have classified all but one of the SCUBA sources with close radio sources, as well as CUDSS 3.2, as having secure identifications. The source we have omitted is CUDSS 3.27, which has two close radio sources. One of these is almost certainly the correct association, but as we are not sure which, we have omitted it from the secure class. We can make a rough estimate of the probability that one of these proposed secure identifications is actually wrong by adding the values of P in Table 2. The total is 0.11, which means the chance of one of these nine secure identifications being wrong is about 10%. Our second class of identifications are suspected identifications. We have placed CUDSS 3.5 in this class. Apart from CUDSS 3.27, we have also placed two other SCUBA sources in this class. For these sources, the statistical evidence that the proposed identification is correct is rather weak, but there is circumstantial evidence, based on the similarity of the colour or structure of the galaxy to known SCUBA galaxies, that the identification is correct (see notes on sources).

5 NOTES ON INDIVIDUAL SOURCES

CUDSS 3.1: This is the brightest source in either of the two CUDSS fields. The object listed in Table 1 has a spectroscopic redshift of 0.1952 (Hammer et al. 1995). There is a tentative $450\mu\text{m}$ detection (W2003), but the $450\mu\text{m}$ position is further from the position of the galaxy than the $850\mu\text{m}$ position. Given the large SCUBA positional errors, it is possible that this galaxy is the counterpart to the SCUBA

Table 2. Identifications

(1) Name	(2) RA (J2000)	(3) Dec (J2000)	(4) Radio, K or I-band	(5) Flux or magnitude	(6) Distance from SCUBA position	(7) <i>P</i>	(8) Status
3.1	03 02 44.84	00 06 32.0	K	19.06±0.02	4.7	0.27	...
3.2	03 02 42.80	00 08 02.5	K	18.64±0.02	1.1	0.021	secure
3.3
3.4	03 02 44.59	00 06 54.9	K	19.64±0.03	2.8	0.21	suspect
3.5	03 02 44.45	00 08 11.1	K	21.4±0.2	0.8	0.08	suspect
3.6	03 02 36.14	00 08 16.8	R	43±12μJy	1.0	0.0006	secure
	03 02 36.14	00 08 16.9	K	21.48±0.21	0.9	0.066	...
3.7	03 02 35.89	00 06 11.5	R	44±12μJy	2.2	0.0029	secure
	03 02 35.90	00 06 12.0	K	20.45±0.09	2.4	0.19	...
	03 02 35.70	00 06 09.5	K	20.54±0.10	1.6	0.11	...
3.8	03 02 26.15	00 06 24.1	R	683±21μJy	7.8	0.038	secure
	03 02 26.16	00 06 24.2	K	14.56±0.003	7.8	0.074	...
3.9	03 02 28.95	00 10 18.6	I	24.23±0.05	0.9	0.12	...
3.10	03 02 52.50	00 08 56.4	R	154±34μJy	1.1	0.00076	secure
	03 02 52.50	00 08 56.4	K	16.31±0.005	1.1	0.0035	...
3.11	03 02 52.85	00 11 22.1	I	25.0±0.4	0.8	0.15	...
3.12
3.13	03 02 36.06	00 09 58.3	K	17.33±0.01	6.1	0.11	...
3.14	03 02 25.68	00 09 06.2	K	20.64±0.23	2.0	0.13	suspect
3.15	03 02 27.73	00 06 53.5	R	226±12μJy	2.2	0.0029	secure
	03 02 27.72	00 06 53.2	K	18.33±0.02	2.0	0.076	...
3.16
3.17	03 02 31.80	00 10 31.2	R	44±12μJy	2.3	0.0033	secure
	03 02 31.52	00 10 28.7	K	18.52±0.03	2.7	0.068	...
3.18
3.19
3.20
3.21
3.22
3.23	03 02 54.06	00 06 18.1	K	20.75±0.26	2.8	0.20	...
3.24	03 02 56.58	00 08 06.6	R	122±32μJy	3.6	0.0082	secure
	03 02 56.57	00 08 06.5	K	19.26±0.07	2.8	0.16	...
3.25	03 02 38.59	00 11 05.3	R	353±12μJy	6.8	0.028	secure
	03 02 38.58	00 11 05.5	K	20.56±0.17	6.5	0.64	...
3.26	03 02 34.92	00 09 10.7	K	19.58±0.09	3.2	0.14	...
3.27	03 02 28.53	00 06 45.0	R	43±12μJy	7.5	0.035	...
	03 02 28.67	00 06 41.2	R	49±12μJy	3.9	0.0097	suspect
	03 02 28.50	00 06 43.2	K	20.27±0.08	5.7	0.62	...

(1) Source name. (2) & (3) Position in J2000 coordinates of the possible counterpart. (4) The waveband in which the possible counterpart was found. An R indicates the counterpart was found on our 1.4 GHz radio image, an I or a K indicate the standard optical/infrared bands. (5) The flux density in μJy of the counterpart if it was found on the radio image; otherwise the I or K-band magnitudes of the counterpart. The errors on the I- and K-band magnitudes do not include the calibration error, which is about 0.05 mags. (6) The distance in arcsec between the position of the possible counterpart and the submillimetre position. (7) The probability that the counterpart is not physically associated with the SCUBA source. (8) Our assessment of the proposed identification based on the criteria described in §4.

Figure 1. Optical (I-band) and near-infrared (K-band) images of the fields. The I-band image is from the Canada-France Deep Field Survey. Each image has a size of 20×20 arcsec², except for the images of CUDSS 3.8, which have a size of 40×40 arcsec². The circle on each image is centred on the SCUBA position and has a radius of 8 arcsec. The near-infrared image has the radio contours superimposed. The five lowest contours are at intervals of 1σ , 2σ , 3σ , 4σ , 5σ (11, 22, 33, 44 and 55 μ Jy), with higher contours being at intervals of 10σ , 20σ , 40σ etc.

Figure 1. —*continued*

source, but the large value for P means that we have no statistical evidence in favour of this possibility.

CUDSS 3.2: This is the one source for which there is some circumstantial evidence that gravitational lensing is important. The redshift estimated for the optical counterpart from the broad-band colours (§9.2) is 0.62, whereas the estimated lower limit to the redshift of the SMS from the lack of a radio

Figure 2. HST I-band images of five of the fields. Each image has a size of 5 arcsec², except for the image of CUDSS 3.8, which has a size of 10 arcsec²

detection (§9.1) is 1.7. The large difference in the redshifts suggests that the SMS is behind the galaxy, with the submillimetre flux being gravitationally amplified by the galaxy (Chapman et al. 2002). The undisturbed morphology of the galaxy (Figure 1) is in agreement with this hypothesis.

CUDSS 3.4: We have classified the galaxy listed in Table 2 as a suspected identification despite the lack of strong statistical evidence from its position and magnitude, for the following reasons. First, the object has a very red colour ($I - K = 4.14$), which qualifies it as an Extremely Red Object (ERO), and SCUBA sources are frequently found to be associated with EROs (Ivison et al. 2000). Second, there is a second much bluer object which is hardly visible on the K-band image but is very prominent on the I-band image (Figure 1). This is actually closer to the SCUBA position (2 arcsec) and has a slightly lower value of P (0.16, calculated from the statistics of the I-band image). There are some faint signs on the CFDF I-band image (Figure 1), although not on the HST image (Figure 2), of an interaction between the two galaxies, which is also a common feature of SCUBA galaxies.

CUDSS 3.5: There are some signs on both the K-band and I-band images that this galaxy has a disturbed morphology. This is a common feature of SCUBA galaxies, and the disturbed morphology adds some circumstantial evidence to the statistical evidence that this is the correct identification. We have classed this galaxy as a suspected identification for the reasons described in §4.

CUDSS 3.6: This is a secure identification, because the position of the SCUBA source is only 1.0 arcsec away from a radio source. The faint object visible on the K-band image (Figure 1) at the radio position has a structure which looks like that of an interacting galaxy.

CUDSS 3.7: On the K-band image there is a distinctive trapezium of sources. The SCUBA source is detected at radio wavelengths, and the radio source is coincident with the

northern of the K-band sources. The northern and southern K-band sources are not detected at all in the CFDF I-band image, and the limits on their $I - K$ colours (> 4.4 and > 4.1) place them in the category of EROs. The eastern K-band source is just visible on the I-band image as the northern of a pair of faint objects. The $I - K$ colour of this source is 3.7, not as red as an ERO but falling within the class of VROs (Very Red Objects) according to the definition of Ivison et al. (2002). The western source is just barely detected in the I-band. The $I - K$ colour is 3.6, making it a VRO. The distinctive arrangement of the sources on the K-band image looks remarkably like a case of gravitational lensing, but the slightly different colours of the sources, and the fact that only one is detected at radio wavelengths, suggests that these sources are not four gravitational images. It therefore seems more likely that the trapezium is actually a cluster of extremely-red high-redshift galaxies.

CUDSS 3.8: Despite the large offset between the radio position and the SCUBA position, there is only a 4% chance that this is a chance coincidence. The peculiar morphology of this galaxy and the fact that it is a strong $15\mu\text{m}$ ISO source (W2003) are compelling evidence that is this the correct identification (§7). The morphology of the system is shown best in the HST image (Figure 2). There are four galaxies and two point sources (presumably stars) visible. Three of the galaxies are spirals. The fourth galaxy has very low surface brightness and is just visible on the western edge of the HST image. The HST image shows that the two brightest galaxies are interacting. The radio image (Figure 1) shows that both of these galaxies are also radio sources. The radio emission is probably the result of starbursts triggered in both galaxies by the interaction. The brightest galaxy has a spectroscopic redshift of 0.088.

CUDSS 3.9: There is nothing visible on the K-band image (Figure 1). There is, however, a faint galaxy visible both on the I-band image from the CFDF survey and on the HST image. The value of P given in Table 2 has been calculated from the statistics of the CFDF I-band image.

CUDSS 3.10: This is a secure identification, with the radio position only 1.1 arcsec away from the SCUBA position. We showed in our previous paper (W2003) that this SCUBA source is also identified with an ISO $15\mu\text{m}$ source, the ISO position also being only 1.5 arcsec from the SCUBA position. There is a bright galaxy coincident with the radio position with a spectroscopic redshift of 0.176 (Hammer et al. 1995). The I-band CFDF image (Figure 1) and especially the HST image (Figure 2) suggest that the galaxy is involved in a merger.

CUDSS 3.11: There is a very faint object visible on the CFDF I-band image (Fig. 1). It is only 0.75 arcsec from the SCUBA position. However, because of the high surface density of objects at this faint magnitude, the probability that it is physically unrelated to the SCUBA source is 15%.

CUDSS 3.14: The probability that the object listed in Table 2, which is 2 arcsec from the SCUBA position, is physically unrelated to the SCUBA source is 13% and therefore above our threshold for a secure identification. We have, however, listed it as a suspected identification because of the other faint objects visible in the CFDF I-band image, some of which are even closer to the SCUBA position. The objects look remarkably like a high-redshift cluster, with

the object listed in Table 2 being the brightest galaxy in the cluster. This is circumstantial evidence in favour of our proposed identification because, as we will show later in this paper (§10), SCUBA galaxies can have optical/near-IR luminosities as high as radio galaxies or first-ranked cluster galaxies.

CUDSS 3.15: This is a secure identification, with a radio source lying only 2 arcsec from the SCUBA position. The source was also detected with ISO at $15\mu\text{m}$ (W2003). On the K-band and CFDF I-band images (Fig. 1) the galaxy looks unexceptional, but the HST image (Fig. 2) shows a ring at the centre of the galaxy, about one arcsec across, encircling a point source. There is also a faint arc on the HST image (labelled a in Figure 2). We cannot decide between two possible interpretations of this system. One possibility is that the object is an example of a ‘collisional ring galaxy’. These objects are thought to be due to the head-on collision between two galaxies, one of which has travelled along the spin-axis of the other, striking the disk of the second galaxy close to its centre (Appleton and Marston 1997). From the multi-band optical and infrared photometry of the identification we estimate that its redshift is $\simeq 0.7$ (§9.2). At this redshift, the physical size of the ring would be typical of those seen in ring galaxies (Appleton and Marston). In this interpretation, the arc seen on the HST image would represent tidal debris from the collision. The alternative interpretation is that the ring and arc represent a gravitational-lensing phenomenon. The size of the ring is approximately what one expect for an Einstein ring produced by a lens with the mass of a typical galaxy. In view of the $15\mu\text{m}$ emission from this galaxy (§7), we suspect the former explanation is the correct one.

CUDSS 3.17: This is a secure identification, with the radio source only 2.3 arcsec from the radio position. However, there is nothing visible on either the I-band or K-band image at the position of the radio source.

CUDSS 3.22: In W2003 we argued that this SCUBA source is identified with a $15\mu\text{m}$ ISO source. The ISO position is 7.5 arcsec from the SCUBA position, and so is indeed within our search radius. However, the two galaxies which are the possible counterparts to the ISO source are both outside the search radius. Indeed, it now seems likely that it is the galaxy which is the furthest from the SCUBA position which is the true counterpart to the ISO source, because this galaxy is also a radio source. We therefore no longer think it is likely that the ISO and SCUBA sources are related. There are a number of possible identifications visible on the CFDF I-band image, but none with a very low value of P .

CUDSS 3.24: This is a secure identification, with a radio source only 3.6 arcsec from the SCUBA position. The galaxy visible at the radio position (Fig. 1) is also a $15\mu\text{m}$ ISO source (W2003). The $I - K$ colour of the galaxy is 3.50, which puts in the category of VROs (Ivison et al. 2002).

CUDSS 3.25: This is a secure identification. The radio source is 6.8 arcsec from the SCUBA position but the probability that this is a chance coincidence is only 3%. The CFDF I-band image shows something which looks like two interacting galaxies, which is circumstantial evidence that the identification is correct.

CUDSS 3.26: The probability of the galaxy being unrelated to the SCUBA source is 14%, and thus the statistical evidence that this is the correct identification is weak.

A piece of circumstantial evidence that this is the correct identification are the different morphologies visible on the I-band and K-band images. The structure on the K-band image extends to the south, suggesting that there may be two objects, a normal galaxy and a very red object which only becomes visible on the K-band image. This is a situation which has been seen for other SCUBA sources (Smail et al. 2002; Chapman et al. 2002).

CUDSS 3.27: This is a rather peculiar field because there are two radio sources, both of which have low values of P , and it is not clear which is the correct identification. We have selected the radio source which is closest to the SCUBA position (and thus has the lowest value of P) as the probable identification. Nevertheless, there are strong circumstantial arguments for the other source being the correct identification because it is both a $15\mu\text{m}$ ISO source (W2003) and the galaxy associated with the source has a disturbed morphology (see the K-band image in Figure 1). The second radio source is, however, much closer to the SCUBA position. There is nothing on either the K-band or I-band images at the position of this radio source.

6 RELIABILITY OF SURVEY

All of the teams carrying out SCUBA surveys have recognised that some of their sources are likely to be spurious, since many of the sources are detected with low signal-to-noise and the surveys are often close to the confusion limit. In earlier papers (Eales et al. 2000; W2003) we estimated that 10% of the CUDSS sources are likely to be spurious, based on both gaussian statistics and on the results of applying our source-detection algorithm to negative maps. Since any SCUBA source with a secure identification is likely to be a genuine submillimetre source, we can use the results of the previous sections to investigate empirically the reliability of the CUDSS survey. In this section we also compare the results of our identification analysis with the results of a similar analysis for the ‘8 mJy’ SCUBA survey, the other large-area blank-field SCUBA survey.

The 8-mJy survey contains 36 sources detected at $>3.5\sigma$ with $850\mu\text{m}$ flux densities ≥ 8 mJy in an area of sky of 260 arcmin^2 (Scott et al. 2002). Thus the survey is less sensitive but covers a larger area than CUDSS. The expected percentage of spurious sources, based on gaussian statistics, is about half the value expected for CUDSS. Ivison et al. (2002) have shown that the fraction of 8-mJy sources with radio associations drops systematically in areas of the original submillimetre images with high noise. They have used this fact to argue that six of the 8-mJy sources are likely to be spurious. After removing these six sources from the catalogue, they find that 60% of the 30 remaining 8-mJy sources are detected at radio wavelengths.

The first thing we can do is compare the percentages of SCUBA sources with radio associations in the two surveys. Nine out of 27 sources in the CUDSS 3-hour field and five out of 23 sources in the CUDSS 14-hour field (Eales et al. 2000; Webb et al. 2003a) have radio detections. These are much lower percentages than are found for the 8-mJy survey. However, the difference can almost certainly be attributed to the different sensitivities, at both submillimetre and radio frequencies, of the different surveys. To show this, we have

compared the radio and submillimetre surveys of the CUDSS 3-hour field with the corresponding 8-mJy surveys. We have excluded the CUDSS 14-hour field because the radio observations were made at 5 GHz, which makes the comparison difficult. Let us assume that the redshift distributions of the objects in the CUDSS and 8-mJy survey are similar. The 8-mJy sources are, on average, a factor of ~ 2 brighter than the CUDSS sources at $850\mu\text{m}$. If the redshift distributions are the same, they will also be brighter by a similar factor at 1.4GHz. To investigate the effects of the flux limits, we have decreased the radio flux of each 8-mJy source (Ivison et al. 2002) by this factor. This decrease now makes the 8-mJy sources directly comparable to the CUDSS. Only seven of the 8-mJy sources now have radio fluxes which fall above the $40\mu\text{Jy}$ limit of our radio observations. Thus the higher percentage of radio detections for the 8-mJy survey is entirely the result of the different flux limits of the two surveys.

We have followed Ivison et al. (2002) in using the statistics of the radio detections to investigate the reliability of the CUDSS survey. Figure 3 shows the fraction of SCUBA sources that are also radio sources as a function of both the signal-to-noise in the original submillimetre survey and of noise in the original submillimetre image. Because of the small number of sources, we have expressed this as a cumulative fraction. In the 3-hour field, the fraction of radio detections clearly does not depend on signal-to-noise. In this field the radio fraction does appear to increase at low values of the submillimetre noise, but since this increase is due to only four out of the 27 sources (of which two are radio detections), we do not regard it as significant. In the 14-hour field, the radio fraction does appear to depend on signal-to-noise but does not depend on the value of the submillimetre noise. Ivison et al. used the result that the radio fraction falls with increasing submillimetre noise in both of the 8-mJy fields to eliminate sources in regions of high noise. Since there is no similar effect which occurs in both of the CUDSS fields, we conclude there is no compelling statistical evidence to eliminate CUDSS sources below some signal-to-noise threshold or in regions of high noise.

A final useful thing we can do with the identification statistics is to derive empirically the distribution of SCUBA position errors. In an earlier paper (Eales et al. 2000), we used a Monte-Carlo simulation to predict the distribution of position errors, but it is preferable to determine these directly. Since the radio positions have an accuracy of better than one arc second, the offset between the radio position and the submillimetre position of a source is a direct measurement of the error in the submillimetre position. There is one caveat to this. If there are errors greater than 8 arcsec, we will miss them, because that was the maximum distance out to which we looked for radio sources (§4). Figure 4a shows the histogram of positional errors for the 14 CUDSS sources with radio detections, overlaid with the distribution of errors predicted from our Monte-Carlo simulation (Eales et al. 2000). The figure shows that in practice our positions are slightly more accurate than the Monte-Carlo simulation predicted. For example, three out of 14 sources (21%) have positional errors ≤ 1 arcsec, whereas our simulation predicted that there would be essentially no sources with position errors this small.

Figure 4b shows the positional errors derived in the same way for the 8-mJy sample (Ivison et al. 2002). In the

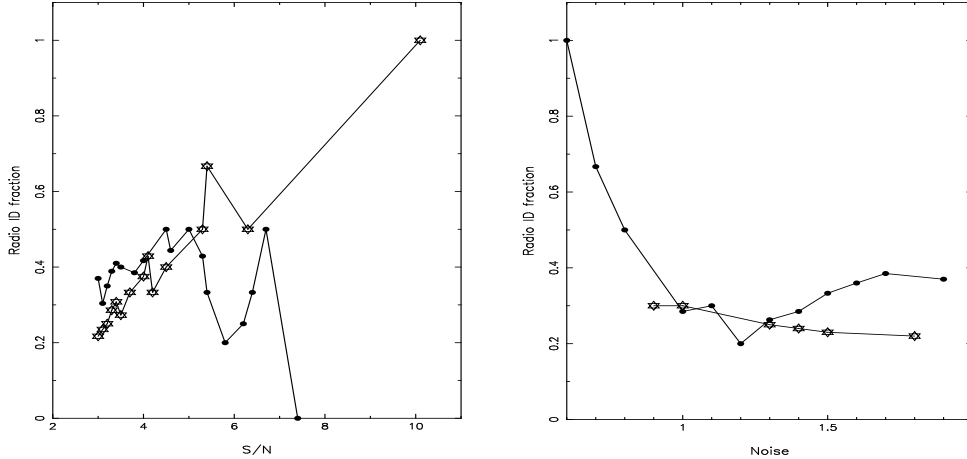


Figure 3. Plots of cumulative fraction of SCUBA sources with radio detections against the signal-to-noise with which a source was detected in the original SCUBA survey (lefthand plot) and against the noise in the original SCUBA survey at the position of the source (righthand plot). The stars represent the results for the 14-hour field, the circles the results for the 3-hour field.

case of the 8-mJy sources, we may be slightly biased towards small positional errors, because the deeper radio data means that a source >4 arcsec from the submillimetre position can not always be confidently associated with the submillimetre source (Ivison et al.). Since the 8-mJy survey is further from the submillimetre confusion limit than the CUDSS, one might expect the accuracy of the positions to be rather better. However, the CUDSS positions are at least as good. For example, five out of 14 CUDSS sources have positional errors ≤ 2 arcsec compared with four out of 18 8-mJy sources. This comparison lends some support to the elaborate, if not very elegant, cleaning technique we used to produce the source catalogue (Eales et al. 2000; W2003).

7 THE IDENTIFICATIONS AT LOW REDSHIFT—GRAVITATIONAL LENSING?

Our identification analysis is based entirely on calculating the probability that an object—either a radio source or a faint galaxy—would fall so close to the position of a SCUBA source if it were actually physically unrelated to the SCUBA source. There is one possible weakness in this approach. If a significant fraction of the SCUBA sources are gravitationally lensed, then it is possible that this technique will find the lens rather than the galaxy which is genuinely responsible for the submillimetre emission. Since the lens will always be at a lower redshift, this method could produce spurious low-redshift identifications for SCUBA sources (Chapman et al. 2002).

The CUDSS contains a larger number of low-redshift identifications than were found in the 8-mJy survey (Ivison et al. 2002). Our small pilot survey at an RA of 10 hours contained two sources which have identifications with spectroscopic redshifts < 1 ($z = 0.074$ and $z = 0.55$, Lilly et al. 1999). The two large fields contain three sources with identifications with spectroscopic redshifts below this limit ($= 0.088$, $z = 0.176$, $z = 0.66$) plus two sources with identifications with estimated redshifts (from the broad-band colours—§9.2) below this limit. Might some of these objects

actually be a lens rather than being the galaxy responsible for the submillimetre emission?

There are three arguments that this is not generally the case. The first of these is described in detail in §9, in which we show that the redshift estimated for the galaxy from multi-band photometry is generally very similar to the redshift estimated for the SMS from the ratio of radio-to-submillimetre flux. The second argument is based on the morphologies of the galaxies. If the galaxies are lenses, they should be galaxies which just happen to fall between the SCUBA source and the Earth, with the only bias in their properties being that they will tend to be galaxies which produce large gravitational amplification factors. There is no reason to expect them to have the morphological peculiarities characteristic of ULIRGs or SCUBA galaxies. However, many of our low-redshift galaxies are indeed extremely peculiar systems. Good examples are the systems of interacting galaxies CUDSS 3.8 and 3.10 (Figure 2).

The third argument is based on the fact that most of the low-redshift identifications are also ISO $15\mu\text{m}$ sources. We have $15\mu\text{m}$ observations of the 3-hour and 14-hour fields but not of the 10-hour field. Of the five low-redshift objects in the former fields, four are detected at $15\mu\text{m}$ (Note that we did not use the $15\mu\text{m}$ results in our identification analysis—§4). The typical shape of the spectral energy distribution of galaxies means that galaxies are unlikely to be detected at $15\mu\text{m}$ at $z \geq 1$ (Eales et al. 2000; Flores et al. 1999). It is therefore unlikely that a SCUBA source at $z \gg 1$ which is being lensed by a low-redshift galaxy will be detected at $15\mu\text{m}$. It is possible that the SMS is being lensed but the $15\mu\text{m}$ emission is from the lens rather than the SMS. By comparing the surface density of $15\mu\text{m}$ sources with the surface density of galaxies with $K < 20$ (Cowie et al. 1994; Flores et al. 1999), we estimate that the probability of a lens also being a $15\mu\text{m}$ source is roughly 10%. Therefore, the probability that four out of five lenses are also $15\mu\text{m}$ sources is clearly extremely low.

One source, CUDSS 3.2, may be the exception that proves the rule. It is the one low-redshift SMS which is

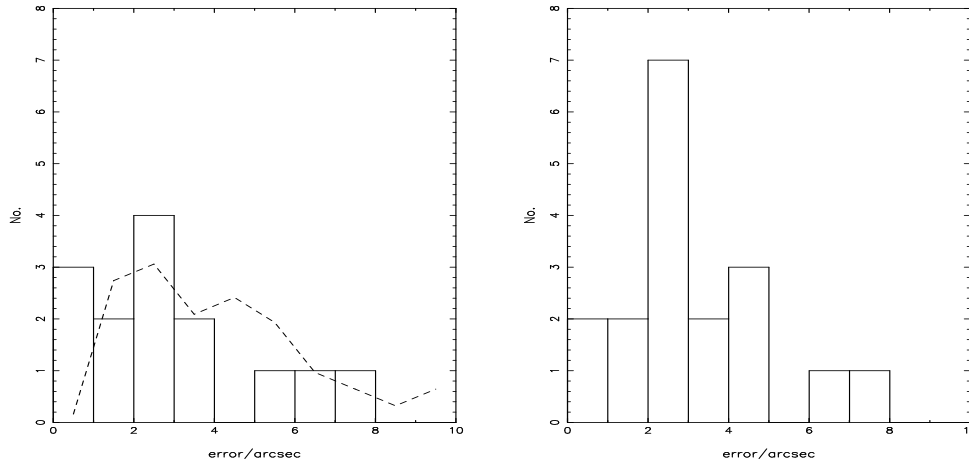


Figure 4. Offsets between the radio and submillimetre positions for submillimetre sources which have radio detections. Since the radio positions are very accurate, these offsets are effectively the errors on the submillimetre positions. The lefthand figure is for the CUDSS. The dashed line shows the prediction we made for the CUDSS positional errors from a Monte-Carlo simulation (Eales et al. 2000). The righthand figure shows the same histogram for the 8-mJy sample, using the data in Ivison et al. (2002).

not detected at $15\mu\text{m}$; the optical counterpart has an undisturbed morphology; and the redshift estimated for the counterpart from multi-band photometry (0.62, §9.2) is much lower than the redshift limit estimated from the ratio of radio-to-submillimetre flux (> 1.7 , §9.1). These properties are all consistent with the hypothesis that the optical counterpart is actually a lens which is gravitationally amplifying the radio and submillimetre emission from an SMS at a much higher redshift. However, the difference in all three respects strongly suggests that the latter SMSs are genuinely at low redshift.

Of the 50 SMSs in the two large fields, there is only one source for which there is plausible evidence for lensing. Blain (1998) predicted that about 2% of SMSs with $S_{850\mu\text{m}} \simeq 10\text{mJy}$ are gravitationally amplified by a factor of ≥ 2 . This is the same as our observed fraction, although the prediction is for a different flux level.

We cannot not use the arguments above for the two sources in the 10-hour field because we have no $15\mu\text{m}$ data for this field. However, both these sources are also detected at $450\mu\text{m}$. Since the ratio of 450 and $850\mu\text{m}$ flux is expected to fall with redshift (Figure 8 of Eales et al. 2000), the detection of these sources at $450\mu\text{m}$ is strong circumstantial evidence that the low-redshift identifications are correct.

If the gravitational-lensing hypothesis can be eliminated, is there any other effect which might produce spurious low-redshift identifications? There is one effect which might be important. At the submillimetre flux level of the CUDSS, the confusion of faint sources is likely to be important. Our Monte-Carlo simulations (Eales et al. 2000) revealed the possible importance of ‘flux-boosting’, in which an apparent single source is actually two or more sources, which are only in the survey because their combined fluxes are greater than the flux limit of the survey. If this is the case for any of our sources, then it is possible that there are two or more genuine identifications close to the submillimetre position, but we have only found the identification at the

lower redshift. There is one possible example of this. CUDSS 3.27 has two possible counterparts, each with a low value of P (§5). In this case, we rejected the counterpart which is detected at $15\mu\text{m}$ because it has a higher value of P than the alternative. But it is possible that both identifications are correct.

Finally, we note that although the fraction of sources with low-redshift identifications is higher in the CUDSS than in the 8-mJy survey, the estimated redshifts of the sources in the 8-mJy survey with submillimetre fluxes below 8mJy is, on average, 0.6 lower than the estimated redshifts of the sources above this flux limit (Ivison et al. 2002). This is additional evidence that the phenomenon that the fraction of sources with low redshifts is increasing as the submillimetre flux limit decreases is a genuine one.

8 THE NATURE OF THE IDENTIFICATIONS—MORPHOLOGIES AND COLOURS

There are 14 secure identifications in the 3-hour and 14-hour fields (this paper and Webb et al. 2003a). Of these, one is not detected at infrared or optical wavelengths, and so it is impossible to classify the morphology of the galaxy; two show no signs of an interaction or have no morphological peculiarity; the remaining 11 show some signs of an interaction or have some peculiarity in the structure. Ivison et al. (2002) performed a similar analysis for the 8-mJy sample. Of the 21 secure identifications, they listed six as being too faint at optical/infrared wavelengths to classify morphologically; 13 as being distorted or close multiple systems; and two as being compact. Given the subjectivity in making classifications of this kind, the proportions seem quite similar in the two surveys.

We are on stronger ground in classifying galaxies according to their colours. Ivison et al. (2002) divided galaxies into EROs ($I-K > 4$) and VROs ($3.3 < I-K < 4.0$). Of 18 SCUBA sources with radio detections, they found that seven

objects had normal colours, 10 objects could be classified as either a VRO or an ERO, and one source was not detected at optical/infrared wavelengths. Of our 14 secure identifications, we find five objects with normal colours, eight objects which are either VROs or EROs, and one object which is not detected at infrared or optical wavelengths. The proportions of objects in the different classes are thus remarkably similar for the two samples.

9 ESTIMATING REDSHIFTS

Chapman et al. (2003a) have recently succeeded in using the Keck Telescope to measure redshifts for 10 SCUBA sources, the first significant number of SCUBA galaxies for which this has been done. However, despite this important success, it is likely that methods for estimating redshifts will be important for several years to come. First, Chapman et al. only targeted SCUBA sources which were detected at radio wavelengths and had I magnitudes $22.2 < I < 26.4$, and thus their results are strictly applicable only to the $\sim 50\%$ of the SCUBA population that satisfy these limits. Since the ratio of radio-to-submillimetre flux is expected to fall with redshift (Carilli and Yun 1999), the radio criterion, in particular, is likely to lead to an underestimate of the proportion of SCUBA sources with $z \geq 2$. Second, Chapman et al. only succeeded in measuring redshifts for about 30% of the sources which satisfied the above criteria. The sources for which they failed may either have weak emission lines or be at a redshift at which emission lines are hard to detect (Chapman et al. noted the relative lack of SCUBA galaxies in the redshift range $1 < z < 2$, the so-called ‘redshift desert’, a redshift interval in which few strong emission lines fall in the optical waveband). For these reasons, methods for estimating redshifts of SCUBA galaxies are likely to continue to be important.

In this section, we investigate two methods for estimating redshifts. Both are well-known but only one has been applied before to SCUBA galaxies. In both cases, we have used the spectroscopic redshifts that do exist for SCUBA galaxies, both from the work of Chapman et al. and from our own work, to test the efficiency of the methods.

9.1 The Radio Method

Carilli and Yun (1999) were the first to point out that for a star-forming galaxy the ratio of radio-to-submillimetre flux should be a function of redshift, and thus that it should be possible to estimate the redshift of a star-forming galaxy from this ratio. Following the original suggestion, a number of groups used different samples of low-redshift objects to determine the expected relationship between this ratio and redshift (Carilli and Yun 2000; Dunne, Clements and Eales 2000; Rengarajan and Takeuchi 2001). There are slight differences between the redshifts estimated using the different sets of low-redshift templates (Ivison et al. 2002).

Figure 5 shows the ratio of submillimetre to radio flux plotted against redshift for all SCUBA galaxies which have both spectroscopic redshifts and radio measurements. We have plotted on the figure the predictions for star-forming galaxies using the 104 low-redshift templates of Dunne, Clements, and Eales (2000). As described in that paper, we

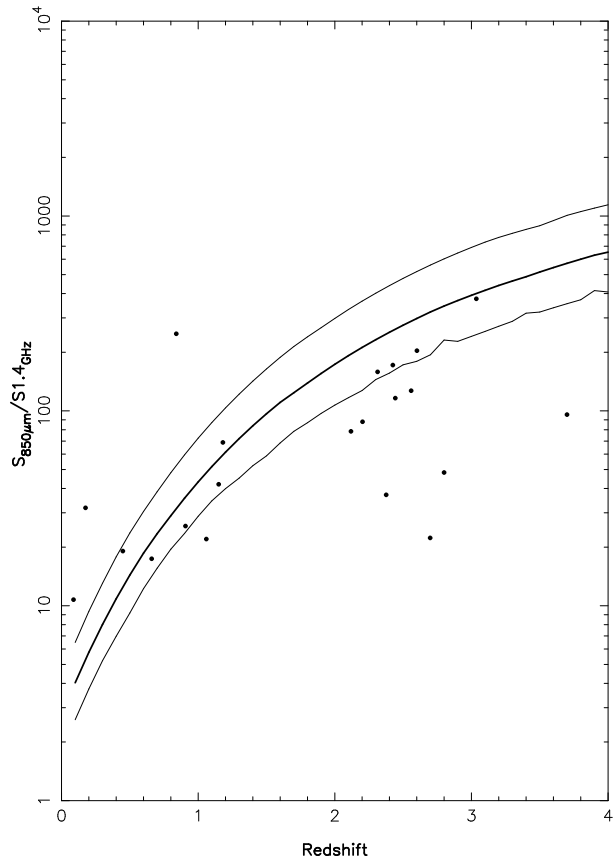


Figure 5. The ratio of $850\mu\text{m}$ flux to 1.4-GHz flux versus redshift. The lines show predictions of how this flux ratio should depend on redshift for star-forming galaxies using the method described in Dunne, Clements and Eales (2000) and in the text. The thick line shows the median prediction of the templates and the thin lines show $\pm 1\sigma$ predictions based on the range of predicted values at each redshift. The points show SMSs with spectroscopic redshifts and radio detections. The data are from Eales et al. (2000), Smail et al. (2000), Ivison et al. (2002), Chapman et al. (2002, 2003), Simpson et al. (2003) and this paper.

first predict the relationship between the flux ratio and redshift for each template and then, at each redshift, determine the median and $\pm 1\sigma$ predicted values. The one slight difference from that paper is that the templates have been modified to incorporate our $450\mu\text{m}$ observations of the galaxies (Dunne and Eales 2001).

At first sight, the diagram does not instill one with much confidence in the method, since for the high-redshift data there is not even a strong correlation between the the flux ratio and redshift. The diagram also suggests that redshifts estimated in this way will generally be underestimates, since nine sources lie below the $\pm 1\sigma$ predictions, while only three sources lie above these predictions. Figure 6 shows the difference between the spectroscopic redshift and the redshift estimated from the median redshift in Figure 5. This figure shows that for about half the SMSs the method works quite well, leading to redshift errors of $z < 0.5$. However, there are also a significant number of SMSs where the method results in a catastrophic redshift error. Similar results are obtained if the other sets of low-redshift templates are used. In Table

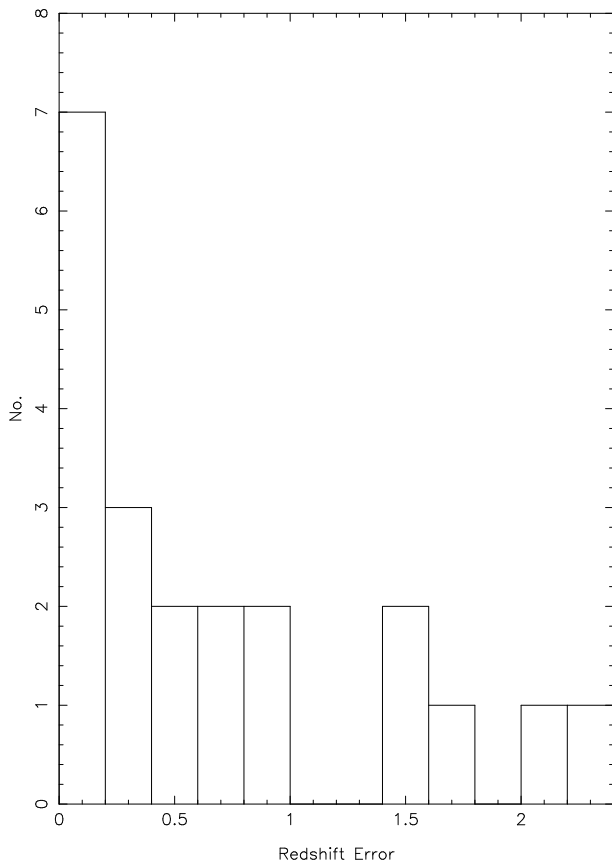


Figure 6. The difference between the spectroscopic redshift and the redshift estimated from the radio method for the 21 SMSs with spectroscopic redshifts and radio measurements. We have estimated the redshift of each SMS using the median prediction in Figure 5.

3 we have listed redshifts estimated in this way for the 15 CUDSS sources with secure identifications.

9.2 Photometric Redshifts

A method which has not been used before to estimate the redshifts for SCUBA galaxies is to use multi-band optical and infrared photometry to estimate ‘photometric redshifts’, a method which was first used extensively in the studies of the Hubble Deep Field. We are in a good position to examine the utility of this method for SCUBA galaxies, because we have observations in five different photometric bands: U, B, V and I photometry from the Canada France Deep Fields and our own K-band photometry. Table 3 lists the multi-band photometry for our 14 secure identifications and multi-band photometry for two other SCUBA galaxies which have spectroscopic redshifts.

We have used the photometric redshift programme of Benitez (2000). Starting from an ensemble of SEDs for low-redshift galaxies, the programme determines the redshift and SED which provide the best fit to the multi-band photometry of the galaxy in question. The attractive feature of the programme is that it uses Bayes theorem to incorporate some prior knowledge about the galaxy population, an approach which reduces the number of ‘catastrophic’ redshift errors. The programme does not incorporate any theoretic-

cal assumptions about galaxy evolution and does not allow for the possibility of dust reddening. However, it is impressively successful at matching the spectroscopic redshifts in the Hubble Deep Field (Benitez 2000) and in the Canada-France Redshift Survey (Waskett et al. 2003b). Table 3 lists the redshifts estimated using this programme.

SCUBA galaxies, of course, must contain large amounts of dust, and thus one might expect any photometric redshift technique to break down when dealing with objects like this. Figure 7 shows the redshift estimates plotted against the spectroscopic redshifts for the six SCUBA galaxies with both spectroscopic redshifts and enough multi-band data to make the photometric technique worth while. The error bars on the photometric redshifts show the redshift range in which there is a probability of 95% that the true redshift lies. For five of the six sources, the agreement between the spectroscopic and photometric redshift is very good, and for the remaining source the disagreement is within the range of the errors. Therefore, although this is a small sample, we conclude that estimating the redshifts of SCUBA galaxies from multi-band photometry is at least as accurate as estimating the redshifts from the ratio of radio-to-submillimetre flux.

Figure 8 shows the two sets of redshift estimates plotted against each other. With the exception of CUDSS 3.2, there is surprisingly good agreement between the two sets, suggesting that for the CUDSS sources we can have some confidence in our redshift estimates. We note that many of the estimated redshifts lie in the so-called ‘redshift desert’, $1 \leq z \leq 2$, a range for which there are no bright emission lines in the optical waveband. It may therefore be quite difficult to measure redshifts for some of these galaxies.

The good agreement between the two sets of redshift estimates is the third piece of evidence that gravitational lensing is not generally important (§7). If lensing were important, there would be no reason why the estimates should agree, since the photometric-redshift method would yield the redshift of the lens and radio-to-submillimetre method would yield the redshift of the lensed object.

10 DISCUSSION

In this section we will discuss what the optical, infrared and radio observations of the CUDSS sources reveal about the nature of SMSs. A later paper will describe an investigation of the evolution of the submillimetre luminosity function which will incorporate the new results.

A simple thing we can do is compare the far-IR—submillimetre luminosities of the CUDSS sources with the luminosities of dust sources in the local universe. A problem which is often skated over in calculating the luminosity of SMSs is that there is usually a flux measurement at only a single wavelength, and therefore the calculation of the luminosity requires some assumption about the SED of the SMS. To investigate the effect of this assumption, we have calculated the luminosity of the CUDSS sources making two different assumptions about the SED. We used two extreme SEDs from the sample of IRAS galaxies of Dunne et al. (2000). NGC 958 is a galaxy whose SED is dominated by cold dust. The observed fluxes of this galaxy are fitted well by the two-component dust model of Dunne and Eales

Table 3. Magnitudes and Redshifts

(1) Name	(2) U_{AB}	(3) B_{AB}	(4) V_{AB}	(5) R_{AB}	(6) I_{AB}	(7) K_{AB}	(8) z_{phot}	(9) z_{spec}	(10) z_{radio}
3.2	23.63 ± 0.05	23.33 ± 0.02	22.63 ± 0.02	...	21.38 ± 0.01	20.55 ± 0.02	0.62 ± 0.21	...	> 1.7
3.6	> 26.98	> 26.38	26.48 ± 0.41	...	> 25.62	23.39 ± 0.21	$1.57^{+0.76}_{-0.46}$...	1.35 ± 0.33
3.7	> 26.98	> 26.38	> 26.40	...	> 26.52	22.36 ± 0.09	2.1 ± 0.6
3.8	20.09 ± 0.01	19.09 ± 0.003	18.25 ± 0.002	...	17.33 ± 0.001	16.47 ± 0.003	0.25 ± 0.16	0.088	0.4 ± 0.18
3.10	21.20 ± 0.01	20.54 ± 0.01	19.07 ± 0.004	...	19.19 ± 0.002	18.22 ± 0.005	0.40 ± 0.18	0.176	0.85 ± 0.23
3.15	24.39 ± 0.07	23.75 ± 0.02	23.31 ± 0.03	...	21.90 ± 0.01	20.24 ± 0.02	0.73 ± 0.23	...	0.6 ± 0.18
3.17	> 26.98	> 26.38	26.48 ± 0.41	...	> 25.62	> 22.84	1.60 ± 0.42
3.24	25.63 ± 0.16	24.85 ± 0.06	24.73 ± 0.08	...	23.22 ± 0.02	21.17 ± 0.07	1.14 ± 0.28	...	1.0 ± 0.25
3.25	25.29 ± 0.14	25.62 ± 0.21	24.72 ± 0.08	...	23.82 ± 0.03	22.47 ± 0.17	$1.05^{+0.27}_{-0.65}$...	0.4 ± 0.18
14.1	27.17 ± 0.32	26.60 ± 0.12	26.28 ± 0.11	...	24.71 ± 0.04	21.18 ± 0.03	1.25 ± 0.3	...	1.9 ± 0.48
14.3	24.71 ± 0.06	24.55 ± 0.03	24.06 ± 0.02	...	23.19 ± 0.01	21.23 ± 0.04	1.11 ± 0.28	...	1.11 ± 0.28
14.9	> 26.98	26.62 ± 0.12	26.40 ± 0.13	...	24.89 ± 0.05	21.12 ± 0.03	1.44 ± 0.32	...	1.7 ± 0.43
14.13	23.93 ± 0.05	23.73 ± 0.02	22.90 ± 0.01	...	20.86 ± 0.004	18.42 ± 0.03	0.90 ± 0.25	1.15	1.2 ± 0.3
14.18	22.97 ± 0.03	22.57 ± 0.01	21.99 ± 0.01	...	20.61 ± 0.003	18.95 ± 0.01	0.69 ± 0.22	0.66	0.7 ± 0.2
N2 850.4 ^a	22.40 ± 0.03	22.47 ± 0.01	22.45 ± 0.02	18.43 ± 0.02	$1.3^{+1.18}_{-0.3}$	2.376	...
N2 850.8 ^a	22.79 ± 0.03	22.68 ± 0.02	22.17 ± 0.02	20.06 ± 0.09	1.41 ± 0.32	1.189	...

(1) Source name. (2)-(7) Magnitudes in the AB system in the different photometric bands. Except where noted, the optical magnitudes are from the Canada-France Deep Fields survey (§3) and the infrared magnitudes are from this paper. In both cases, the errors on the magnitudes do not include the calibration error, which is about 0.05 mags. (8) Redshift estimated using the photometric redshift method of Benitez (2000). (9) Spectroscopic redshift. (10) Redshift estimated from the ratio of radio-to-submillimetre flux. Notes on sources: a—The data for these objects were taken from Ivison et al. (2002).

(2001), with dust at 20K and 44K in the ratio by mass of 186:1. At the other extreme is the galaxy IR1525+36, which, in the Dunne and Eales model, has dust at 19K and 45K in the ratio by mass of 15:1. Figure 9 shows the luminosities of the CUDSS sources with secure identifications calculated using these two different assumptions. We have also plotted in the figure the luminosities of the IRAS galaxies in the sample of Dunne et al. (2000). For the CUDSS galaxies without spectroscopic redshifts, we have used the redshift estimated from our multi-band photometry (§9.2) and, if that is not possible, the redshift estimated from the ratio of radio and submillimetre flux (§9.1). The figure shows that there is roughly a factor of five difference in the luminosities of the CUDSS sources calculated with the two different SEDs, showing the sensitivity of the calculation to the assumption about the SED. With the cold SED, there is a substantial overlap in the luminosities of the CUDSS sources with the low-redshift sample, although the majority of the CUDSS sources are still more luminous than the most luminous object in the local sample, the archetypical ULIRG Arp 220.

Given our extensive multi-band optical/IR photometry, we can calculate the ratio of dust luminosity to optical/IR luminosity. For each source with a secure identification, we calculated the optical/IR flux by integrating the observed SED from 0.25 to $2.5\mu\text{m}$. We estimated the flux at each wavelength by making a power-law interpolation between the two neighbouring photometric measurements. The biggest uncertainty in this calculation is the question of which SED to use to calculate the dust luminosity. Figure 10 shows the histogram of dust luminosity divided by optical/IR luminosity, with the dust luminosity calculated using the cold SED. The figure shows that most of the CUDSS sources have dust luminosities which are between 10 and 100

times greater than emission in the optical/near-IR bands. If the hot SED is used to calculate the dust luminosities, these figures increase by a factor of about five. Whichever SED is used, figures 9 and 10 show that, as one would expect, the CUDSS sources are luminous systems with most of the emission being reprocessed emission from dust.

We now compare the absolute magnitudes of the SMSs with those of other high-redshift objects. Dunlop (2002) plotted the K magnitudes of SMSs against their redshift and compared this diagram to the same diagram for radio galaxies, which are among the most luminous galaxies known. By comparing the apparent magnitudes of SMSs and radio galaxies at the same redshift, he was able to compare the absolute magnitudes of the two types of object. He concluded that the host galaxies of SMSs have absolute magnitudes which are very similar to those of radio galaxies. At redshifts < 3 , the K-band falls on the long-wavelength side of the 4000\AA break, and thus the K-band light is not dominated by the light from young stars but rather by the light from the stars that form most of the stellar mass of a galaxy. Therefore, one inference which one might draw from Dunlop's result is that the host galaxies of SMSs are giant galaxies in which a large fraction of the stars have already formed.

A limitation of this study, however, was that at that time there were only three SMSs with spectroscopic redshifts. These were also SMSs which were known to be gravitationally lensed, which means there is necessarily some uncertainty in the value of the gravitational amplification factor. Because there are now a significant number of SMSs with spectroscopic redshifts, we can now carry out a much more extensive comparison of the magnitudes of SMSs with the magnitudes of other high-redshift objects.

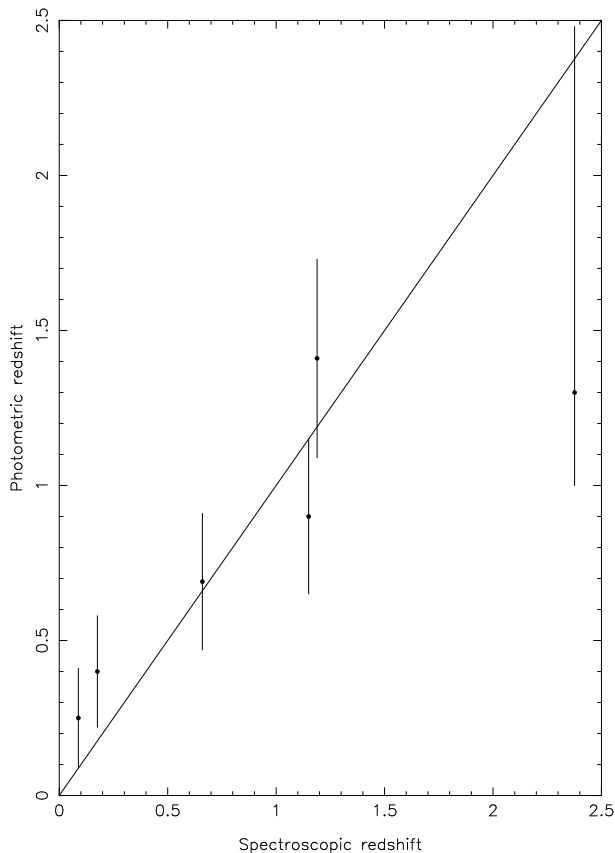


Figure 7. Spectroscopic redshift versus photometric redshift for the six galaxies with extensive multi-band photometry and spectroscopic redshifts. The spectroscopic redshift is equal to the photometric redshift along the line.

Figure 11 shows K magnitude plotted against redshift for (a) all SMSs with spectroscopic redshifts which are not known to be lensed and (b) all CUDSS sources with secure identifications. For the CUDSS galaxies without spectroscopic redshifts, we have used the redshift estimated from our multi-band photometry (§9.2) and, if that is not possible, the redshift estimated from the ratio of radio and submillimetre flux (§9.1). We have also plotted on the diagram the data for radio galaxies described in Eales et al. (1997). In order to ensure that there are no spurious differences caused by magnitudes being measured in apertures of different sizes, we have corrected all the magnitudes to a common metric aperture. Most of the magnitudes for the SCUBA galaxies have been measured through a 3-arcsec aperture, which at $z = 2$ is equivalent, with our cosmological assumptions (§1), to a physical distance of 23.5 kpc. We have converted the photometry for the radio galaxies to this metric aperture using the method described in Eales et al. (1997). The figure confirms Dunlop’s conclusion that many SMSs have host galaxies which are as luminous as radio galaxies. About half the SMSs are, however, in host galaxies which are fainter than radio galaxies, although the difference is usually small enough that they must still be fairly luminous systems.

Another interesting population with which to compare the SMSs are the galaxies found in μJy radio surveys. The morphologies of these radio sources (Muxlow et al. 2003) suggest the emission is generally from a star-forming disk rather

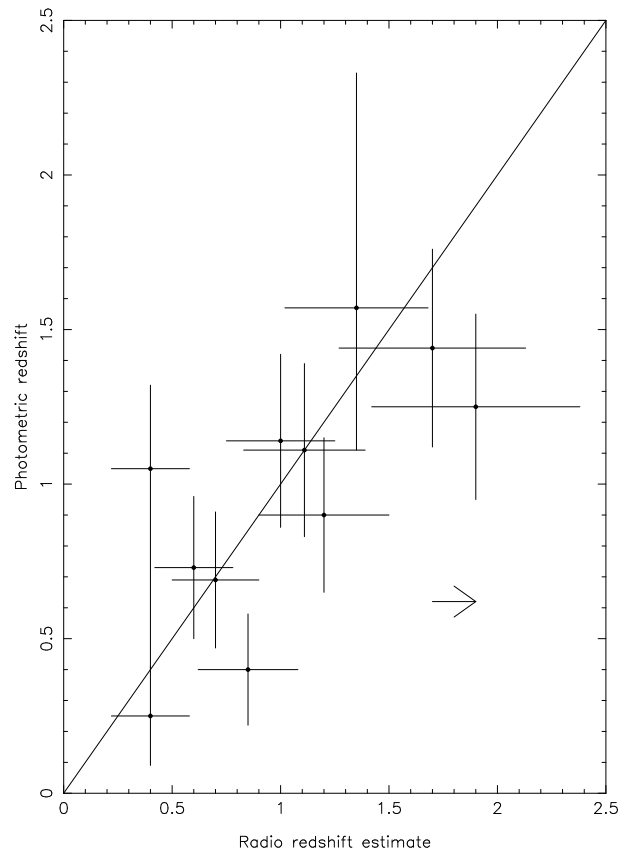


Figure 8. Redshift estimated from the multi-band optical and infrared photometry versus redshift estimated from the radio-to-submillimetre flux ratio. The arrow is CUDSS 3.2, which has an upper limit for its radio flux.

than being the result of an active nucleus, as is the case for the classical radio galaxies plotted in the figure. Chapman et al. (2003b, and references therein) have carried out a multi-wavelength study of these sources. A significant fraction of them are also detected in the submillimetre waveband, and Chapman et al. argue that there is a substantial overlap between the μJy population and the SMSs. They have also found the interesting result that the optical absolute magnitudes of the μJy radio sources have a small range, with most of host galaxies having an optical luminosity fairly close to L_* . They speculate that the reason for this may be that less luminous, and therefore less massive, galaxies are less efficient at confining cosmic rays.

We have taken the median I-band absolute magnitude and $I - K$ colour given in Chapman et al. to estimate the median K -band absolute magnitude, which we have then used to predict a $K - z$ relationship for these objects. This is shown in the figure. It passes neatly through the middle of the SMS points, which suggests that the host galaxies of SMSs and μJy radio sources are very similar in their optical/IR luminosities. The colours of the two classes are also quite similar. The median $I - K$ colour of the CUDSS sources with secure identifications is 3.3, very similar to the value of 3.4 given by Chapman et al. for the optically-faint μJy radio sources. Therefore, both the colours and the optical/IR luminosities of the host galaxies are additional pieces

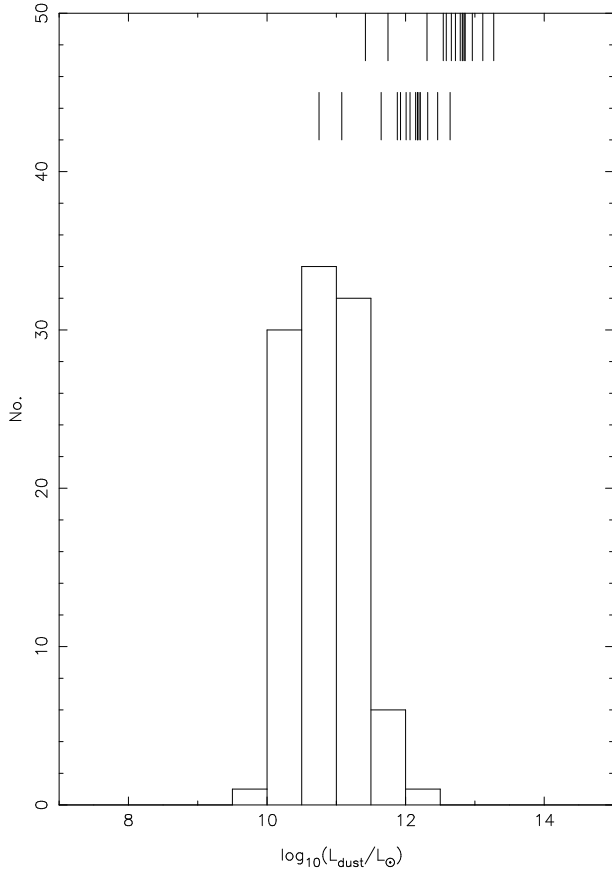


Figure 9. The far-IR—submillimetre luminosities of the CUDSS sources with secure identifications and of the IRAS galaxies in the sample of Dunne et al. (2000). The histogram shows the luminosities of the IRAS galaxies. The lower set of vertical lines mark the luminosities of the CUDSS sources calculated using the SED of NGC 958 (see text); the upper set of lines show the luminosities calculated using the SED of IR1525+36.

of evidence that there is, at the least, a substantial overlap between the two populations.

It might be thought that the identification of SMSs with luminous galaxies is an argument against these objects being at an early stage of galactic evolution, since a large number of stars have clearly already formed. This is not necessarily so. Simple models of the evolution of dust in a galaxy (Dunne, Eales and Edmunds 2003, and references therein) imply that the mass of dust in a galaxy will be at a maximum when roughly half the stars are formed. With the caveat that the submillimetre luminosity also depends on dust temperature, the time when the dust mass is at its greatest will also be the time at which the submillimetre luminosity is at its peak. How close this time is to the time at which star formation started in the galaxy depends on the characteristic timescale of star formation. If most of the stars form in a burst, as may well be the case for elliptical galaxies, the interval between the onset of star formation and time when half the stars have formed may be very short indeed. If these ideas are correct, then the SMSs plotted in the figure will be roughly a factor of two more luminous in the optical/near-IR waveband by the current epoch.

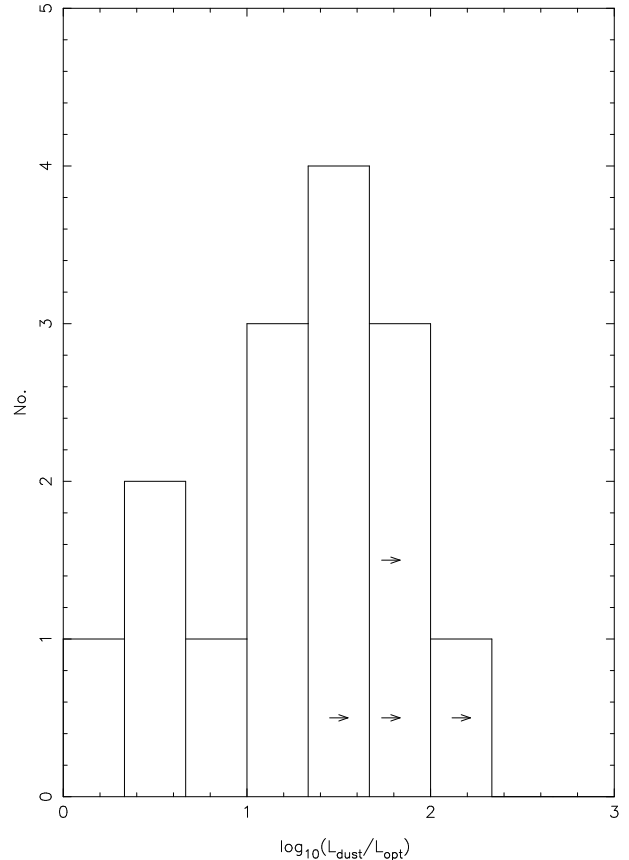


Figure 10. Histogram of the ratio of dust luminosity to optical/IR luminosity for the CUDSS sources with secure identifications. We have calculated the dust luminosity using the SED of NGC 958 (see text). The lower limits are for sources which have not yet been detected in the optical/IR.

11 CONCLUSIONS

We have presented optical, near-infrared and radio observations of the 3-hour field of the Canada-UK Deep Submillimetre Survey. We have reached the following conclusions:

- (1) Of the 27 submillimetre sources in this field, 9 have secure identifications with either a radio source or a near-IR source. Of the 50 submillimetre sources in the two CUDSS fields, 14 now have secure identifications.
- (2) The percentage of sources with secure identifications is consistent with that found for the bright 8-mJy submillimetre survey, once allowance is made for the different submillimetre and radio flux limits.
- (3) Of the 14 secure identifications, eight are VROs or EROs, five have colours typical of normal galaxies, and one is a radio source which has not yet been detected at optical/IR wavelengths. These proportions are very similar to those found for the 8-mJy survey. Eleven of the identifications have optical/near-IR structures which are either disturbed or have some peculiarity which suggests that the host galaxy is part of an interacting system, a similar percentage to that found for the 8-mJy survey.
- (4) We have examined the reliability of the CUDSS catalogue. In contrast to the result of a similar analysis for the 8-mJy survey, we find no clear evidence that CUDSS

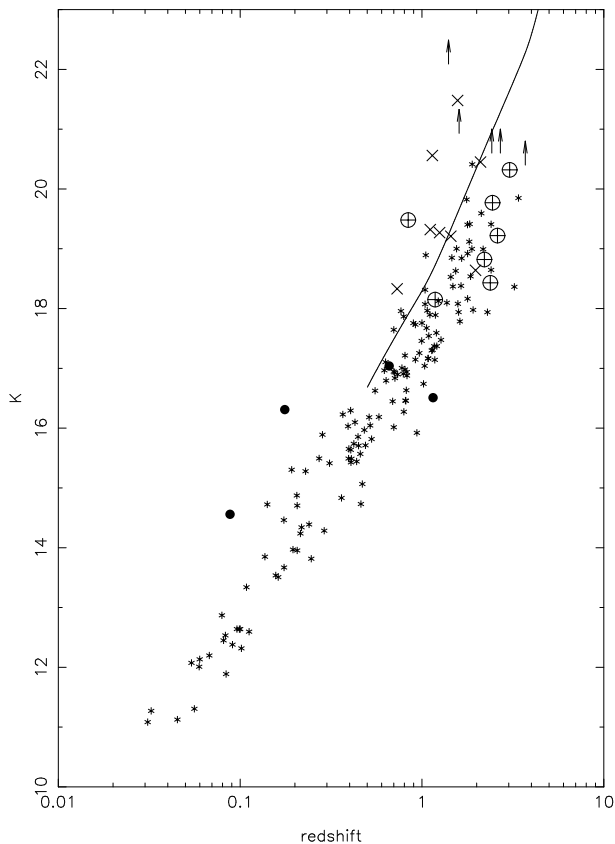


Figure 11. K-band magnitude versus redshift for SCUBA galaxies and radio galaxies. The stars show the positions of the samples of radio galaxies described in Eales et al. (1997). The other symbols represent SMSs. The filled circles are for CUDSS sources with secure identifications and spectroscopic redshifts. The crosses-in-circles show other SMSs with spectroscopic redshifts (Chapman et al. 2003a). The crosses represent CUDSS sources with secure identification but only estimated redshifts (see text). The lower limits are for SMSs with secure identifications with radio sources but which are undetected in the K band. Three of these have spectroscopic redshifts (Chapman et al. 2003a), and two of these are CUDSS sources for which we have estimated redshifts from the ratio of radio and submillimetre flux. The line shows the predicted relation for μ Jy radio sources (see text).

sources with low S/N or at positions in the submillimetre maps where the noise is high are any less reliable than the rest of the sources.

(5) We have critically examined different methods of estimating the redshifts of SMSs. We show that the method of estimating redshifts from the ratio of radio and submillimetre flux (Carilli and Yun 1999) works well for about 50% of SMSs, but there are a significant number of catastrophic errors. We show the method of estimating redshifts from the multi-band optical and near-IR photometry works surprisingly well.

(6) We conclude that the low-redshift identifications are genuine low-redshift submillimetre sources rather than being gravitational lenses. This conclusion is based on (i) the morphologies of the identifications, (ii) the good agreement between the photometric redshifts of the galaxies and the redshifts estimated from the ratio of radio to submillimetre

flux, (iii) the fact that the majority of the low-redshift identifications are also $15\mu\text{m}$ sources.

(7) We show that many SMSs are in host galaxies which are as bright in the near-IR as radio galaxies, which are among the most luminous galaxies in the universe. However, on average, the host galaxies of SMSs are slightly less bright in the near-IR than the classical radio galaxies. They are, however, very similar, in both their absolute near-IR/optical magnitudes and colours, to the host galaxies of the radio sources detected in μ Jy radio surveys.

ACKNOWLEDGMENTS

Research by DC, SAE, RI, WKG is supported by the Particle Physics and Astronomy Research Council. SAE thanks the Leverhulme Trust for the award of a research fellowship during a critical phase in this research. LD is supported by a PPARC fellowship and KW by a PPARC studentship.

REFERENCES

- Alexander, D.M. et al. 2003, *AJ*, 125, 383.
 Almaini, O. et al. 2003, *MNRAS*, 339, 397.
 Appleton, P.N. & Marston, A.P. 1997, *AJ*, 113, 201.
 Barger, A.J. et al. 1998, *Nature*, 394, 428.
 Benitez, N. 2000, *ApJ*, 536, 571.
 Bertoldi, F. et al. 2000, *A & A*, 360, 92.
 Bertoldi, F., Menten, K.M. Kreysa, E., Carilli, C.L. & Owen, F. 2001, 24th meeting of the IAU, Joint Discussion 9, Manchester, England (astro-ph 0010553).
 Blain, A.W. 1998, *MNRAS*, 297, 502.
 Blain, A.W., Kneib, J.-P., Ivison, R.J. & Smail, I. 1999, *MNRAS*, 512, 87.
 Brinchmann, J. et al. 1998, *ApJ*, 499, 112.
 Carilli, C.L. & Yun, M.S. 1999, *ApJ*, 513, L13.
 Carilli, C.L. & Yun, M.S. 2000, *ApJ*, 530, 618.
 Chapman, S.C., Smail, I., Ivison, R.J. & Blain, A.W. 2002, *MNRAS*, 335, L17.
 Chapman, S.C., Blain, A.W., Ivison, R.J. & Smail, I.R. 2003, *Nature*, 422, 695.
 Chapman, S.C. et al. 2003, *ApJ*, 585, 57.
 Cole, S., Lacey, C.G., Baugh, C.M. & Frenk, C.S. 2000, *MNRAS*, 319, 168.
 Cowie, L.L., Gardner, J.P., Hu, E.M., Songaila, A., Hodapp, K.-W. & Wainscoat, R.J. 1994, *ApJ*, 434, 114.
 Downes, A.J.B., Peacock, J.A., Savage, A. & Carrie, D.R. 1986, *MNRAS*, 218, 31.
 Dunlop, J.S. 2002, *A New Era in Cosmology*, ASP Conference Series, eds T. Shanks and N. Metcalfe, astro-ph 0203183.
 Dunne, L., Clements, D. & Eales, S. 2000, *MNRAS*, 319, 813.
 Dunne, L., Eales, S., Edmunds, M., Ivison, R., Alexander, P. & Clements, D. 2000, *MNRAS*, 315, 115.
 Dunne, L. & Eales, S. 2001, *MNRAS*, 327, 697.
 Dunne, L., Eales, S. & Edmunds, M. 2003, *MNRAS*, 341, 589.
 Eales, S.A., Rawlings, S., Law-Green, D., Cotter, G. & Lacy, M. 1997, *MNRAS*, 291, 593.
 Eales, S.A., Lilly, S., Gear, W., Dunne, L., Bond, J.R., Hammer, F., Le Fèvre, O. & Crampton, D. 1999, *ApJ*, 515, 518.
 Eales, S.A., Lilly, S., Webb, T., Dunne, L., Gear, W., Clements, D. & Yun, M. 2000, *AJ*, 120, 2244.
 Eggen, O., Lynden-Bell, D. & Sandage, A. 1962, *ApJ*, 136, 748.
 Flores, H. et al. 1999, *ApJ*, 517, 148.
 Flores, H. et al. 2003, in preparation.

- Gear, W.K., Lilly, S.J., Stevens, J.A., Clements, D.L., Webb, T.M., Eales, S.A. & Dunne, L. 2000, MNRAS, 316, 51.
- Hammer, F., Crampton, D., Le Fèvre, O. & Lilly, S.J. 1995, ApJ, 455, 88.
- Hogg, D.W. 2001, AJ, 121, 1207.
- Hughes, D.H. et al. 1998, Nature, 394, 241.
- Ivison, R. et al. 2000, MNRAS, 315, 209.
- Ivison, R.J. et al. 2002, MNRAS, 337, 11.
- Larson, R.B. 1975, MNRAS, 173, 671.
- Lilly, S.J., Le Fèvre, O., Crampton, D., Hammer, F. & Tresse, L. 1995, ApJ, 455, 50.
- Lilly, S., Eales, S., Gear, W., Hammer, F., Le Fèvre, O., Crampton, D., Bond, J.R. & Dunne, L. 1999, ApJ, 518, 641.
- McCracken, H.J., Le Fèvre, O., Brodwin, M., Foucaud, S., Lilly, S.J., Crampton, D. & Mellier, Y. 2001, A&A, 376, 756.
- Muxlow, T. 2003, in preparation.
- Percival, W.J., Scott, D., Peacock, J.A. & Dunlop, J.S. 2003, MNRAS, 338, L31.
- Rengarajan, T.N. & Takeuchi, T. 2001, PASJ, 53, 433.
- Richards, E.A. 2000, ApJ, 533, 611.
- Scott, S. et al. 2002, MNRAS, 331, 817.
- Serjeant, S. et al. 2003, MNRAS, in press (astro-ph 0201502).
- Simpson, C. et al. 2003, in preparation.
- Smail, I., Ivison, R.J. and Blain, A.W. 1997, ApJ, 490, L5.
- Smail, I., Ivison, R.J., Owen, F.N., Blain, A.W. & Kneib, J.-P. 2000, ApJ, 528, 612.
- Smail, I., Owen, F.N., Morrison, G.E., Keel, W.C., Ivison, R.J. & Ledlow, M.J. 2002, ApJ, 581, 844.
- Smail, I., Chapman, S.C., Ivison, R.J., Blain, A.W., Takata, T., Heckman, T.M., Dunlop, J.S. & Sekiguchi, K. 2003, submitted to MNRAS (astro-ph 0303128).
- Sutherland, W. and Saunders, W. 1990, MNRAS, 259, 413.
- Waskett, T. et al. 2003a, MNRAS, 341, 1217.
- Waskett, T. et al., in preparation.
- Webb, T., Lilly, S.J., Clements, D.L., Eales, S.A., Yun, M., Brodwin, M., Dunne, L. & Gear, W.K. 2003a, ApJ, in press.
- Webb, T. et al. 2003b, ApJ, 587, 41.
- Webb, T., Eales, S., Lilly, S.J., Clements, D.L., Dunne, L., Gear, W.K., Flores, H. & Yun, M. 2003b, ApJ, 587, 41 (W2003).

This figure "Fig1a.jpg" is available in "jpg" format from:

<http://arxiv.org/ps/astro-ph/0312269v1>

This figure "Fig1b.jpg" is available in "jpg" format from:

<http://arxiv.org/ps/astro-ph/0312269v1>

This figure "Fig2.jpg" is available in "jpg" format from:

<http://arxiv.org/ps/astro-ph/0312269v1>